PROCEEDINGS OF SCIENCE

Prospects of non-resonant and resonant Higgs pair production at the HL-LHC

Amit Adhikary,[a,*] **Shankha Banerjee,**[b] **Rahool Kumar Barman,**[c] **Biplob Bhattacherjee**[d] **and Saurabh Niyogi**[e]

[a] *Institute of Theoretical Physics, Faculty of Physics, University of Warsaw, Pasteura 5, PL 02-093, Warsaw, Poland*

[b] *CERN, Theoretical Physics Department, CH-1211 Geneva 23, Switzerland*

[c] *Department of Physics, Oklahoma State University, Stillwater, Oklahoma, 74078, USA*

[d] *Centre for High Energy Physics, Indian Institute of Science, Bangalore 560012, India*

[e] *Gokhale Memorial Girls' College, 1/1, Harish Mukherjee Road, Kolkata 700020, India*

E-mail: amit.adhikary@fuw.edu.pl

We combined multiple final states ensuing from non-resonant Higgs pair production by optimising over each final state using multivariate techniques and put bounds on the self-coupling of Higgs by employing the log-likelihood confidence level hypothesis test. Further, we calculate the production cross-section limits from multifarious heavy Higgs decay channels, including resonant di-Higgs production, in a model-independent way and draw its impact on the MSSM parameter space at the HL-LHC.

**** The European Physical Society Conference on High Energy Physics (EPS-HEP2021), ****
**** 26-30 July 2021 ****
**** Online conference, jointly organized by Universität Hamburg and the research center DESY ****

*Speaker

https://pos.sissa.it/

PoS(EPS-HEP2021)610

1. Introduction

The measurement of Higgs boson self-coupling is among the next goal of the Large Hadron Collider (LHC) era. It can verify the nature of Higgs potential and thereby the electroweak symmetry breaking (EWSB) mechanism. However, a direct measurement of this coupling requires an observation of Higgs pair or di-Higgs production, $pp \to hh$. This observation becomes challenging because of the small di-Higgs production rate in Standard Model (SM). At the LHC, the dominant production happens via the gluon fusion process with a triangle and box diagram, and there is destructive interference between these two diagrams. Our motive is to analyse various Higgs pair production channels at the HL-LHC and infer the potential of HL-LHC in di-Higgs observation [1].

We are now aware of beyond the SM (BSM) physics which is a requirement to understand various unexplained phenomena in SM. One such well-motivated BSM model to explore new particle searches is the Minimal Supersymmetric Standard Model (MSSM). We investigate the Higgs sector of MSSM in our work [2]. Here, we specifically search for MSSM Higgs bosons in various final states and evaluate the reach of HL-LHC in the MSSM parameter space.

2. The non-resonant Higgs pair production

Here, the term "non-resonant" refers to the Higgs pair production in SM. Multifarious Higgs decay modes constitute phenomenologically rich di-Higgs final states. We select the final states which are clean (containing photons or leptons) and has appreciable production rates, *viz.* $b\bar{b}\gamma\gamma$, $b\bar{b}\tau\tau$, fully leptonic and semi-leptonic $b\bar{b}WW^*$ and $WW^*\gamma\gamma$, and the $4W$ channel with 2, 3 and 4 lepton final states. We simulate the di-Higgs signal in these channels and the corresponding background processes in `MG5_aMC@NLO` [3]. The generated processes are showered and hadronised via `Pythia` [4]. These events are passed to `Delphes-3.4.1` [5] for the detector simulation.

We perform a cut-based and multivariate analysis using Boosted Decision Tree (BDT) algorithm in the TMVA framework [6] in all the aforementioned di-Higgs channels. The $b\bar{b}\gamma\gamma$ channel contains photons in the final state. This channel has the disadvantage of $h \to \gamma\gamma$ branching ratio but has a clean signature at the collider. The QCD-QED $b\bar{b}\gamma\gamma$ process is the dominant background in this channel. We first do the cut based analysis where one of the kinematic variables is the invariant mass of the bottom pair, m_{bb}. The kinematic distribution of m_{bb} is shown in Fig. 1. The black curve corresponds to the di-Higgs signal, and others are the backgrounds. A cut of 100 GeV $< m_{bb} <$ 150 GeV is applied to separate signal from backgrounds. We use 14 kinematic variables constructed from the final state during BDT analysis, and the final result improves about 20% compared to the previous cut-based analysis.

Next, we analyse the $b\bar{b}\tau\tau$ channel where we divide the final state according to the leptonic or hadronic decays of τ's. The di-τ mass reconstruction is crucial in this channel because of the neutrinos in the final state. We use the collinear mass approximation technique to reconstruct the $h \to \tau\tau$ leg. The kinematic distribution of this variable, $M_{\tau_h\tau_h}$, is shown in Fig. 1. In case of $b\bar{b}WW^*$ and $WW^*\gamma\gamma$ final states, we divide them into fully-leptonic and semi-leptonic channels. The dominant background contribution comes from the $t\bar{t}$ and $t\bar{t}h$, $h \to \gamma\gamma$ process, respectively. In Fig. 1, the m_{ll} and ΔR_{lj} corresponds to one of the best kinematic variables during the BDT analysis in $b\bar{b}WW^*$ and $WW^*\gamma\gamma$ channels, respectively. We further analyse the WW^*WW^* channel in three final states, *viz.* same-sign di-lepton channel: $\ell^\pm\ell^\pm + 4j + \not{E}_T$, 3-lepton channel: $3\ell + 2j + \not{E}_T$ and 4-lepton channel: $4\ell + \not{E}_T$. The final states with more leptons suffer from the event rates, while with more jets the QCD backgrounds become huge. In the same-sign di-lepton channel, we perform a BDT analysis and one best kinematic variable, $\Delta R_{l_1 j_2}$, is shown in Fig. 1.

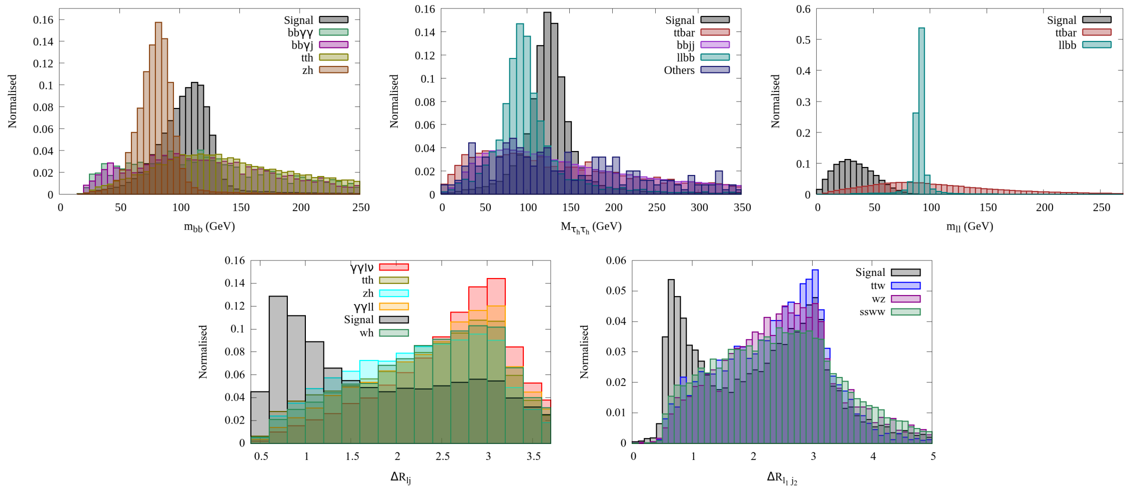

Figure 1: The normalised kinematic distributions for one of the best variables in various di-Higgs final states. The kinematic variables m_{bb}, $M_{\tau_h\tau_h}$, m_{ll}, ΔR_{lj} and $\Delta R_{l_1 j_2}$ are taken from $b\bar{b}\gamma\gamma$, $b\bar{b}\tau\tau$, $b\bar{b}WW^*$, $WW^*\gamma\gamma$ and $4W$ final states, respectively. The black curve corresponds to the signal process, $gg \to hh$. These distributions show the efficiency of these variables in distinguishing signal from the background processes.

Various non-SM or new physics (NP) might affect the di-Higgs production in many ways. One of them is via changing the self-coupling of Higgs boson. A deviation from the SM Higgs self-coupling value is quantified as the ratio of the measured value and the SM value of Higgs self-coupling, $\kappa = \lambda/\lambda_{SM}$. We analyse the best channel $b\bar{b}\gamma\gamma$ by selecting $\kappa = -1, 1, 2, 5$ and 7. Here, $\kappa = 1$ corresponds to the SM Higgs self-coupling. The kinematics changes upon changing the κ from SM value, which can be seen in Fig. 2 for $p_{T,\gamma\gamma}$ distribution. After using the BDT optimisation of $\kappa = 1$ for all other values of κ, the log-likelihood confidence level (CL) hypothesis test [7] puts a limit of $-0.63 < \kappa < 8.07$ at 95% CL.

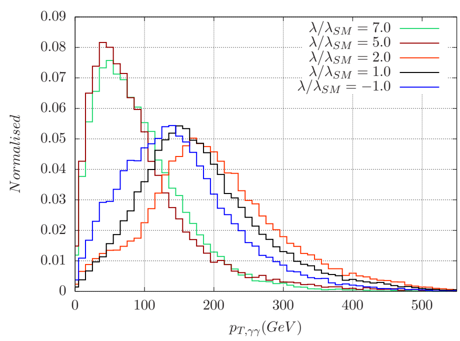

Figure 2: The normalised distribution of $p_{T,\gamma\gamma}$ in the $b\bar{b}\gamma\gamma$ channel for different values of λ/λ_{SM}.

3. The resonant Higgs pair production

The Higgs sector in many BSM models includes additional Higgs bosons and the 125 GeV Higgs boson. We consider a well-motivated BSM model, called MSSM, which contains two CP even (h, H), one CP odd (A) and two charged $(H^{\pm})$ Higgs bosons. Here, the lightest CP even scalar, h, is the SM-like Higgs boson. Our objective is to analyse the heavy Higgs (H, A) decays, put upper limits (UL) on their production rates in a model-independent way and constrain the MSSM parameter space.

The following final states are considered in the analysis, *viz.* $pp \to H \to hh$, $pp \to H \to t\bar{t}$ and $pp \to b\bar{b}H, H \to \tau\tau$. Here, the first decay channel of heavy Higgs, $pp \to H \to hh$, is called resonant Higgs pair production. We select the following resonant di-Higgs decay modes, *viz.* $b\bar{b}\gamma\gamma$, $b\bar{b}b\bar{b}$, $b\bar{b}\tau\tau$, $b\bar{b}WW^*$ and $\gamma\gamma WW^*$. The main advantage is the resonant peak in the kinematic distribution, as compared to the previous non-resonant di-Higgs production (section 2). A comparison is shown for resonant process with various heavy Higgs masses and the non-resonant di-Higgs process at the leftmost plot of $p_{T,\gamma\gamma}$ in Fig. 3. In case of the $b\bar{b}\gamma\gamma$ channel, we do a cut-based analysis where we optimise over $m_{b\bar{b}\gamma\gamma}$ and $p_{T,\gamma\gamma}$ variables. Two plots on the right of Fig. 3 shows their kinematic distribution. The solid and dashed lines correspond to signal and backgrounds, respectively. We put model independent upper limits on the $\sigma(pp \to H \to hh)$, at 95% CL. These limits are shown in Fig. 4 without (left) and with 5% (right) systematic uncertainty. The limit is stronger below and above around $m_H = 600$ GeV for the $H \to hh \to b\bar{b}\gamma\gamma$ and $H \to hh \to b\bar{b}b\bar{b}$ channel, respectively.

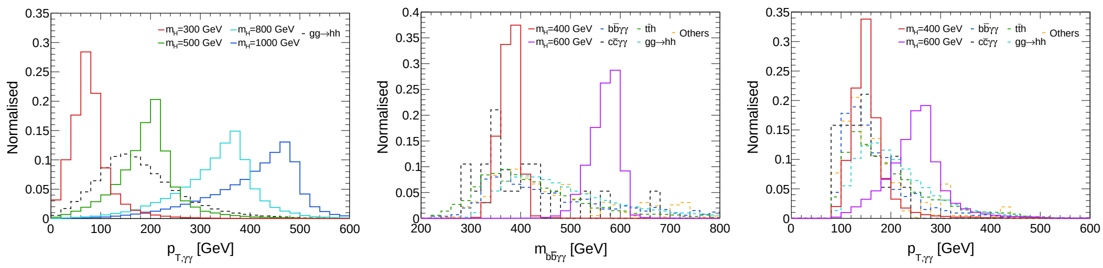

Figure 3: The leftmost distribution shows the difference in $p_{T,\gamma\gamma}$ between the resonant (with m_H = 300, 500, 800, 1000 GeV) and non-resonant Higgs pair production. The two distributions on the right corresponds to the best kinematic variables in the $pp \to H \to hh \to b\bar{b}\gamma\gamma$ final state, *viz.* $m_{b\bar{b}\gamma\gamma}$ and $p_{T,\gamma\gamma}$.

In case of $pp \to H \to t\bar{t}$ channel, the dominant background comes from $t\bar{t}$ process. Here, the final state for signal and background is similar $(t\bar{t})$ and this leads to difficulty in the signal-background separation unless we reconstruct the resonant $H \to t\bar{t}$. This reconstruction is possible in case of the semi-leptonic channel where the only source of missing transverse energy, $\not{E}_T$, is the leptonically decaying W boson. We get two possible invariant masses, $m_{t\bar{t}1}$ and $m_{t\bar{t}2}$, for the two possible solutions of neutrino p_z. They are shown in Fig. 5. These variables perform better during the BDT analysis. The semi-leptonic $H \to t\bar{t}$ final state puts stronger UL on $\sigma(pp \to H \to t\bar{t})$ varying in the range $\sim$ [187, 33] fb for m_H = [400, 1000] GeV. Finally, the $pp \to b\bar{b}H, H \to \tau\tau$ final state gives 95% CL upper limit on $\sigma(pp \to b\bar{b}H) \times Br(H \to \tau\tau) \sim$ [22, 4] fb between m_H = [300, 500] GeV.

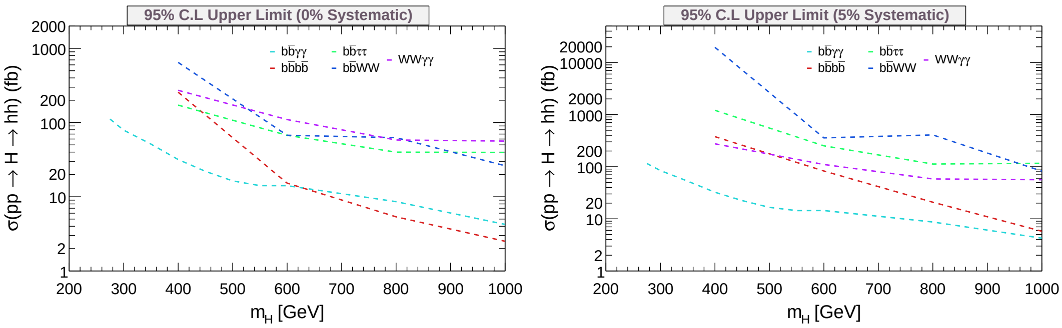

Figure 4: The 95% CL upper limit placed on the resonant di-Higgs production cross-section for various final states without (left) and with 5% (right) systematic uncertainty.

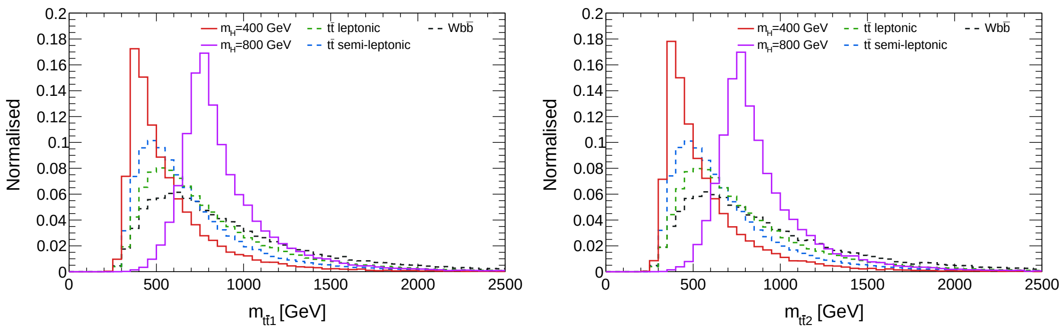

Figure 5: The invariant mass distribution reconstructed from the pair of top-quarks in the $H \to t\bar{t}$ (semi-leptonic) channel. The $m_{t\bar{t}1}$ and $m_{t\bar{t}2}$ correspond to the $t\bar{t}$ invariant mass from two possible solutions of neutrino transverse momentum in the semi-leptonic channel.

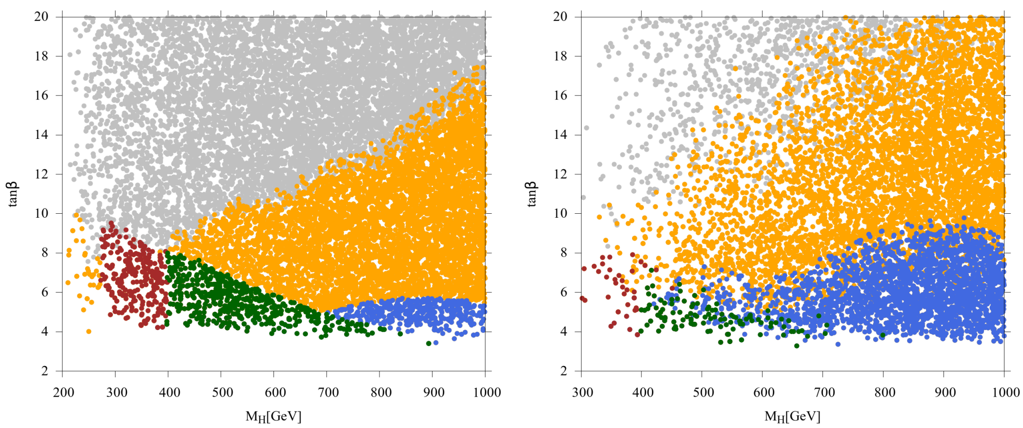

Figure 6: Projected HL-LHC reach for heavy Higgs decaying to only SM final states (left) and SM+supersymmetic decays (right) in the $m_A - \tan\beta$ plane.

Next, we translate the 95% CL upper limits into projected reach in the $m_A - \tan\beta$ plane, where m_A is the pseudoscalar Higgs mass and $\tan\beta$ is the ratio of two vacuum expectation values of the two Higgs doublets in MSSM. In Fig. 6, the left plot shows the HL-LHC reach for the heavy Higgs searches. ATLAS and CMS Run-II data (36 fb^{-1}) excludes the grey coloured points via search in the $pp \to b\bar{b}H/A, H/A \to \tau\tau$ channel. The HL-LHC can constrain the brown, green and orange coloured points at 95% CL via searches in $H \to hh \to b\bar{b}\gamma\gamma$, $H \to t\bar{t}$ and $b\bar{b}H, H \to \tau\tau$ final states, respectively. While the blue coloured points will evade these limits. These limits become weaker in the presence of non-SM decay modes of heavy Higgs boson, for example, heavy Higgs to neutralino/chargino decay, which is shown on the right in Fig. 6.

4. Summary

We have explored many di-Higgs final states, including better performing channels and the less-studied final states. The $WW^*\gamma\gamma$ channel has a good signal over background ratio, so that this channel might become important with higher energy colliders. Although a higher energy collider will be better in Higgs self-coupling measurement, we can get an improved result at the HL-LHC by combining several Higgs pair production final states and combining the results from both the ATLAS and CMS collaboration. We further performed heavy Higgs searches at the HL-LHC and put limits in the $m_A - \tan\beta$ plane. The $pp \to H \to hh$ and $pp \to H \to t\bar{t}$ final state can probe the low m_A and low $\tan\beta$ region, whereas the high $\tan\beta$ region can be probed via the $pp \to b\bar{b}H, H \to \tau\tau$ channel. These limits get modified in the presence of non-SM heavy Higgs decays.

References

[1] A. Adhikary, S. Banerjee, R. K. Barman, B. Bhattacherjee and S. Niyogi, Revisiting the non-resonant Higgs pair production at the HL-LHC, JHEP 07 (2018) 116

[2] A. Adhikary, S. Banerjee, R. K. Barman and B. Bhattacherjee, Resonant heavy Higgs searches at the HL-LHC, JHEP 09 (2019) 068

[3] J. Alwall, R. Frederix, S. Frixione, V. Hirschi, F. Maltoni, O. Mattelaer et al., The automated computation of tree-level and next-to-leading order differential cross sections, and their matching to parton shower simulations, JHEP 07 (2014) 079

[4] T. Sjostrand, S. Ask, J. R. Christiansen, R. Corke, N. Desai, P. Ilten et al., An Introduction to PYTHIA 8.2, Comput. Phys. Commun. 191 (2015) 159–177

[5] DELPHES 3 collaboration, J. de Favereau, C. Delaere, P. Demin, A. Giammanco, V. Lema^ıtre, A. Mertens et al., DELPHES 3, A modular framework for fast simulation of a generic collider experiment, JHEP 02 (2014) 057

[6] A. Hoecker, P. Speckmayer, J. Stelzer, J. Therhaag, E. von Toerne, H. Voss et al., TMVA - Toolkit for Multivariate Data Analysis, ArXiv Physics e-prints (Mar., 2007), [physics/0703039]

[7] T. Junk, Confidence level computation for combining searches with small statistics, Nucl. Instrum. Meth. A 434 (1999) 435, [hep-ex/9902006]